A Study of Oceanic Boundary-Layer Characteristics Including Inertial Oscillation at Three Drifting Stations in the Arctic Ocean

MILES G. MCPHEE

U.S. Army Cold Regions Research and Engineering Laboratory, Hanover, NH 03755

(Manuscript received 3 September 1979, in final form 4 February 1980)

ABSTRACT

Measurements of surface drift and near-surface currents taken during August 1975, at drifting ice stations of the AIDJEX experiment in the central Arctic, are used to infer the response of the upper ocean to the passage of two frontlike wind events. As an aid in interpretation, a multilevel, time-dependent, dynamical boundary-layer model commensurate with earlier investigations of PBL turbulence and ice drift versus surface wind statistics is developed and shown to reproduce the main features observed, including energetic inertial oscillation of the ice cover and mixed layer, relatively small currents at 30 m (~5 m into the pycnocline), and little inertial-period shear between the ice and currents measured at 2 m. The model employs an eddy viscosity dependent on the surface friction velocity (u_*) and the nondimensional depth (fz/u_*) in the well-mixed layer, and on the product of the local stress and the local Obukhov length in the upper pycnocline. When the dominant horizontal length scale (related to the Coriolis parameter and the propagation speed of the atmospheric system) is of the order 750 km, the phase and amplitude of the inertial motions across the 190 km span of the station array are observed to be more coherent than predicted by the locally driven (i.e., horizontally homogeneous) model. It is suggested that a small pressure term due to Ekman convergence could account for the discrepancy.

1. Introduction

The physics of the planetary boundary layer (PBL) that develops under pack ice drifting under the influence of surface winds has been elucidated in a series of experiments performed in the Arctic over the past decade. Smith (1974) described the evolution of a successful technique for measuring mean flow and the fluctuating (Reynolds) stress tensor at several levels through the mixed layer and upper pycnocline using small current meters mounted in orthogonal triplets. McPhee and Smith (1976, hereafter MS) showed how, with proper scaling, the resulting turbulence measurements were similar to those predicted by neutrally buoyant PBL models developed for the atmosphere (e.g., Deardorff, 1972; Wyngaard *et al.*, 1974). The appropriate scales were u_*, u_*^2 and u_*/f for velocity, kinematic stress and vertical length, respectively; here u_* is the surface layer friction velocity and f the Coriolis parameter. We also inferred a distribution of eddy viscosity through the PBL by examining the vertical distribution of wavenumbers associated with peaks in the spectra of vertical velocity fluctuations. From that we concluded that a simple *dimensionless* eddy viscosity formulation, such as one suggested by Businger and Arya (1974), might be useful for parameterizing turbulent stress in the upper ocean as well as the atmosphere.

The experiments in which turbulent stress was measured occurred during winter conditions (i.e., when the ice was compact and, because of its comparatively high strength, capable of modifying significantly the transfer of momentum from the wind to the ocean). This probably accounted for the fact that observations of surface-driven currents were relatively free of inertial-period oscillations, contrary to most observations in open ocean mixed layers. We were naturally curious about how turbulent structure might change in the presence of energetic inertial motion. During the summer melt season (mid-July to mid-September) of 1975, four drifting stations of the AIDJEX main experiment in the central Arctic did experience sizable inertial oscillations as indicated by cycloidal loops in their drifting trajectories and by inertial waves in velocity records from suspended current meters. We showed (McPhee, 1978a, hereafter M1) that these motions occurred in response to rapid changes in surface wind by relating the surface (ice) velocity to the total ice-ocean PBL transport, which was obtained by solving a simple bulk momentum equation driven by the observed wind. In its essential features, the approach is similar to the "slab" model of Pollard and Millard (1970) in that both use a depth integral of the momentum equation to circumvent the problem of how turbulent momentum transfer happens within the boundary layer.

Subsequently (McPhee, 1979a, hereafter M2) we

0022-3670/80/060870-15$07.75

investigated the statistical relationship between surface stress, surface drift velocity and near-surface currents during the 1975 melt season, exploiting the fact that internal ice forces were then small. The main purpose of M2 was to find, from 60 days of smoothed drift and wind records at four camps, a statistical expression for surface stress in terms of ice velocity. We found that the observed expression for stress magnitude in terms of surface speed was not linear, as it would have been for constant eddy viscosity K_m and was not quite quadratic as it would have been for constant nondimensional eddy viscosity, fK_m/u_*^2; instead it followed a form indistinguishable from that required by Rossby number similarity, thus corroborating the earlier turbulence measurements (MS). We then showed that this expression compared favorably with a similar relationship from a specific first-order PBL model patterned after that of Businger and Arya (1974).

During August 1975, two eastward propagating atmospheric systems crossed the AIDJEX array, setting up rapid drift with inertial oscillations at all the camps. In this paper, we present an analysis of upper ocean response to these specific wind events. The work is a sequel to MS and M2 in that we interpret the oceanic response in terms of a multilevel, time-dependent model of stress in the PBL using a first-order closure assumption and a relatively simple eddy viscosity distribution based on mixed layer measurements and plausible scaling in the upper pycnocline.

The proposed model, as indeed do most oceanic boundary-layer treatments (e.g., Mellor and Durbin, 1975; Kondo *et al.*, 1979), assumes horizontal homogeneity, i.e., that the local forcing is uniform over a large enough area to make horizontal variations in the boundary-layer properties unimportant. Obviously, this assumption is open to question: one can imagine times when local forcing at locations, say, 200 km apart would tend to excite inertial waves that are completely out of phase. Such forcing would induce divergence in the boundary-layer transport, which via local pressure-gradient terms could become significant in the momentum balance, and provide an important link between boundary-layer forcing and excitation of inertio-gravity waves in the stratified interior ocean, as explored theoretically by Krauss (1972, 1976). Thus it is useful to ask how gradients in a particular wind field, which are related to how fast the system moves, affect the response of the oceanic boundary layer. The measured evolution of inertial wavetrains across the 190 km span of the manned array, combined with high quality surface wind data, provide a rare opportunity to address this question. Therefore, we shall compare the kinematics of the observed inertial motions with the purely local simulations.

The paper is arranged as follows. In the next section, wind and drift data are introduced. In Section 3 the previous steady-state boundary-layer model (Businger and Arya, 1974; M2) is extended to include time dependence and a more realistic pycnocline treatment. A detailed simulation of measured surface, 2 m and 30 m currents is presented, along with a discussion of stress, shear and turbulent kinetic energy at selected levels in the model. In Section 4 the simulated inertial component of drift at three stations is compared with observed data, followed by a discussion of horizontal gradients. Section 5 is a brief summary.

2. Observations of two inertial events

Fig. 1 shows the configuration and mean drift of the AIDJEX manned stations from 7 August 1975 (day 219) to 19 August 1975 (day 231). Stations are identified by the initials of their radio call names—from west to east: Snowbird (SB), Caribou (CA), Big Bear (BB) and Blue Fox (BF). Data collected routinely at each camp included 1) Navy Navigation Satellite (NAVSAT) positioning with each fix accurate to within 40 m; 2) surface (10 m) wind, including inertial subrange estimates of wind stress; 3) continuous current records (relative to the drifting ice) at nominal depths of 2 m and 30 m below the ice; and 4) daily salinity-temperature-depth (STD) casts to ~700 m.

For the purposes of the AIDJEX ice modeling project, the NAVSAT position data were originally processed with a Kalman filtering technique designed to achieve maximum accuracy over time scales of about a day using translocation techniques. The filter provided evenly spaced (3 h) samples of position, velocity and acceleration, but was estimated by Thorndike and Cheung (1977) to attenuate roughly half of the power in the velocity record at the inertial period. Because of this relatively poor response near the inertial peak, we tested the earlier transport model (M1) by estimating the inertial ice motion from the current shear between the surface and 30 m. This seemed plausible because of a sharp pycnocline beginning a few meters above the 30 m level at all the camps, and appeared to work well enough for the main camp (BB). However, a comparison of the long-term measured 30 m currents and the ice drift across the array showed large variation among the current meters from camp to camp (McPhee, 1978b). This, combined with the results of field calibrations in early 1976, indicated fairly large errors in the current meter records at two camps (SB and BF); thus the current shear approach was of limited value for tracing the inertial signal over the whole array.

Since that time, the NAVSAT data have been reprocessed with a higher frequency-response filter to take advantage of the fact that up to 30 fixes per

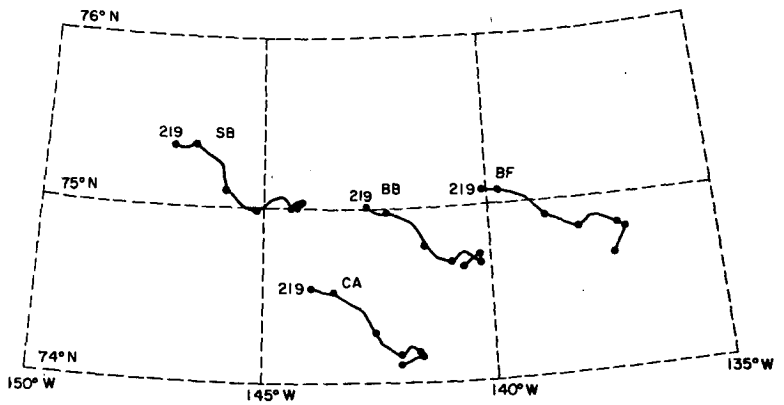

FIG. 1. Location and approximate drift trajectories of AIDJEX manned stations, 7 August 1975 (day 219) to 19 August 1975 (day 231).

day were obtained at each camp. The newly processed records give much better resolution of the inertial motions most of the time. (Some caution is required in their interpretation since the original sampling was not uniform in time and the filter smooths over data gaps, but these gaps can be identified by looking at the frequency of the original fixes, as examples below will show).

Fig. 2 shows hourly average components of surface wind at the four camps arranged in ascending order from west to east during a 12-day period spanning the passage of two sharp frontal events on days 221 and 225. The coordinate system is such that the y axis points north along the 142°W meridian, so that u and v are approximately zonal and meridional components, respectively.

By noting arrival times, we infer that the first event was traveling eastward at ~60 km h^{-1}. For the most part, the storm retained its basic character as it traversed the array, an exception being the sharp southward spike occurring at SB early on day 222, which is much less pronounced by the time it reaches BF.

The second storm behaved differently. If we estimate its arrival time by tracing the almost discontinuous front in the eastward component passing SB at day 225.5, it appears to be moving only about half as fast as the first. There is also more change in the storm itself as it passes the array; for example, the northward spike passing SB at 225.5 has become more diffuse by the time it reaches BF. We can thus anticipate that there may be differences in the inertial motions initiated by the two events.

Fig. 3 shows the drift velocity of the camps in the same format as Fig. 2. It is clear that the storms set off energetic inertial oscillations. A central supposition of this paper is that these oscillations

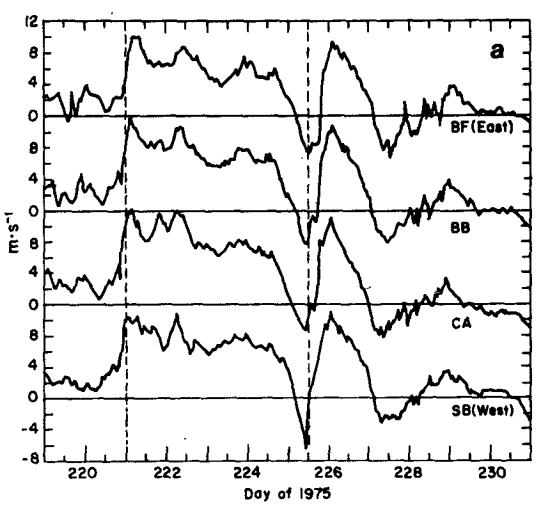

FIG. 2a. Eastward component of surface (10 m) wind during observing period.

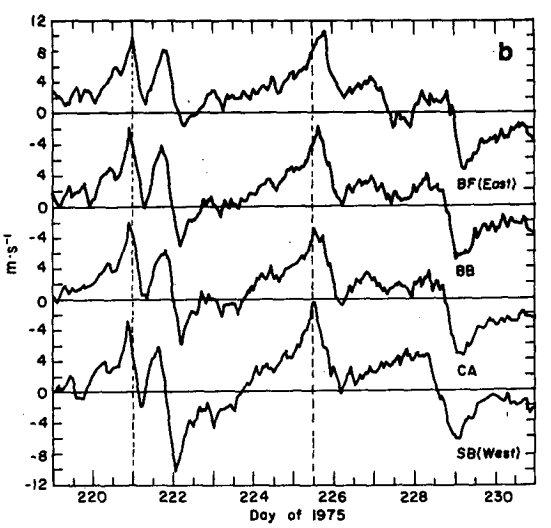

FIG. 2b. As in Fig. 2a except for northward component.

are predominantly a boundary-layer effect, and the pack ice enters the problem only as its mass modifies the wind stress. In a previous analysis (McPhee, 1980), we showed evidence that this is true for low frequencies (periods of a day and longer) during a relatively short (two month) melt season, and here we assume that it holds for all frequencies.

Since traces shown in Fig. 3 are the output of the filtering technique mentioned above, they have been smoothed where gaps in the NAVSAT record occurred. For example, there was a 17 h gap at BB after 225.5 which accounts for the anomalously smooth curve then. There were also important interruptions in CA's record: 16 h beginning about 221.5 and others after day 226 and again after day 229. In the case of CA (but not BB) lapses in the position record were accompanied by gaps in surface wind data; for this reason, we excluded CA from further analysis. Fortunately, SB, BB and BF were spread in longitude in a fairly narrow latitude band, so that to the extent that the wind systems propagated zonally, this was the optimum arrangement of three stations.

In addition to surface velocity, currents were measured at nominal depths of 2 m and 30 m at all camps. A description of the apparatus and initial data processing is given by McPhee (1978b). For that report, the current meter data were filtered to remove inertial period motion. The following observations about low-frequency currents are pertinent. First, the main signal seen at 30 m is the ice motion. The actual current is obtained by subtracting the vector ice velocity from the current

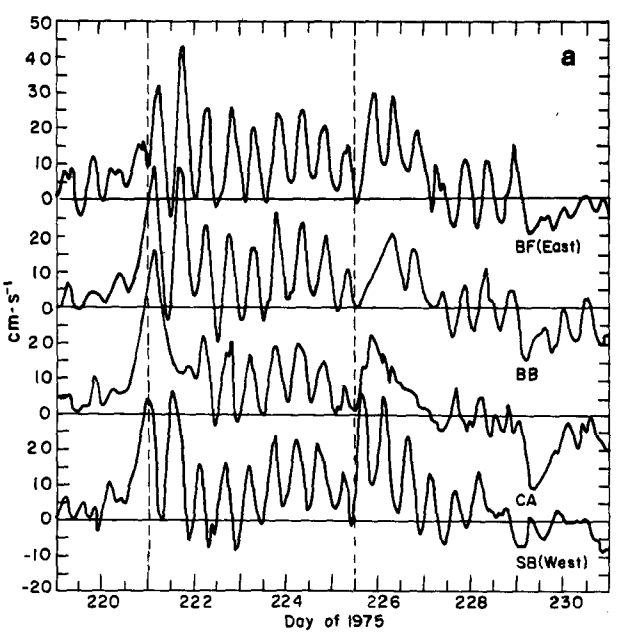

FIG. 3a. Eastward component of station drift velocity from NAVSAT positions.

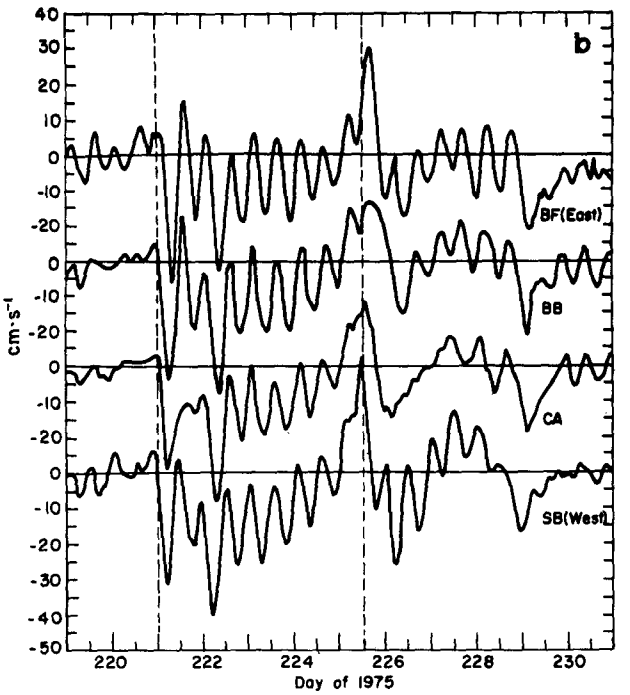

FIG. 3b. As in Fig. 3a except for northward component.

measured relative to the ice. Since these vectors are of comparable magnitude, a highly accurate current meter system is required to find the absolute current. Second, as mentioned earlier, we suspect sizable long-term errors in the 30 m current meters, both from *in situ* calibrations and from the fact that the raw data imply unacceptably large divergence in the mean flow at 30 m. Nevertheless, there is probably a good deal to be gained by considering the current data, particularly at higher frequencies; therefore we applied an *ex post facto* calibration procedure suggested in the data report: namely, for each camp we applied a constant scaling and rotation to the relative 30 m currents such that the mean absolute current for the 20-day period 221–241 was zero. The actual current at that level is thought to be less than 3 cm s^{-1}; thus the object is to reduce errors in the large inertial signals to something of that order. The scale factors and rotation angles are as given in Table 1 of McPhee (1978b). No corrections were applied to the 2 m currents, since they were generally more consistent from camp to camp (but there were unexplained variations in relative direction—see Table 4 of M2).

One further item to consider regarding the current meter records is that logbook entries from field observers sometimes mentioned sizable frame deflections during periods of fast drift. This implies a maximum departure of as much as 10% of nominal depth (R. Parmentier, personal communication), which may have been a significant

proportion of the distance from the density interface to the 30 m level. The effect is mentioned for completeness only; no explicit account of it was taken in light of other current meter errors.

3. The numerical model and local simulations

The time-dependent boundary-layer model is an extension of a steady-state atmospheric PBL model introduced by Businger and Arya (1974) and subsequently adapted by the author (M2) to relate observations of average ice drift to surface winds during the 1975 melt season, when internal ice forces were negligible. Our intent is to use it to simulate the inertial motions described in Section 2 and the currents observed with suspended current meters.

While in some respects the model is perhaps too simplistic, we have tried not to grossly compromise experimental evidence gathered in previous ice-floe projects. This has required some modification to the original model, most notably in the treatment of density stratification as described below; still our philosophy has been to keep the complexity of the theory somewhat commensurate with our ability to test it, which means that our main objective is to simulate surface drift and currents measured at 2 and 30 m.

a. The stress equation

The basic approach is described in M2. The momentum equation is closed at first order by relating the turbulent stress in the fluid to the gradient of mean velocity by means of a similarity eddy momentum exchange coefficient. In nondimensional terms, the horizontally homogeneous component equations in a reference frame drifting with the surface geostrophic current (assumed constant) are

$$\frac{\partial u}{\partial t} - v = \frac{\partial T^x}{\partial \xi}, \tag{1}$$

$$\frac{\partial v}{\partial t} + u = \frac{\partial T^y}{\partial \xi}, \tag{2}$$

where

$$(u,v) = \left(\frac{\hat{u}}{u_*}, \frac{\hat{v}}{u_*}\right), \quad t = f\hat{t},$$

$$(T^x,T^y) = \left(\frac{\tau^x}{u_*^2}, \frac{\tau^y}{u_*^2}\right), \quad \xi = \frac{fz}{u_*}.$$

Here $(\hat{u},\hat{v})$ is the mean dimensional current relative to the surface geostrophic flow, where "mean" is taken in the sense that $(\hat{u},\hat{v})$ varies slowly compared to the turbulent fluctuations responsible for the kinematic, turbulent Reynolds stress (τ^x,τ^y). The friction velocity u_* is the square root of stress at the ice-ocean interface and $\hat{t}$ is dimensional time.

The closure assumption is

$$(T^x,T^y) = K_*\left(\frac{\partial u}{\partial \xi}, \frac{\partial v}{\partial \xi}\right), \tag{3}$$

with $K_* = fK_m/u_*^2$, K_m being the dimensional eddy viscosity.

Eqs. (1) and (2) are differentiated with respect to ξ and (3) is substituted to obtain coupled time-dependent stress equations

$$\left.\begin{aligned} T^x_t - T^y &= K_* T^x_{\xi\xi} \\ T^y_t + T^x &= K_* T^y_{\xi\xi} \end{aligned}\right\}, \tag{4}$$

where subscripts indicate differentiation and the simplifying assumption has been made that terms involving temporal changes in K_* are small compared to inertial terms. We found in MS that the time scale of the energy-containing eddies was of the order of a few minutes; thus the turbulent field adjusts rapidly to surface conditions and we assume that K_* reflects this instantaneously.

b. The K_* distribution

The crux of the model is the prescription of K_*. As reviewed in M2 for the neutrally stable PBL, a simple analytic expression (where k is von Kármán's constant)

$$K_* = -k\xi e^{c_1\xi}, \quad \xi < 0, \tag{5}$$

has the desirable properties of increasing almost linearly with depth close to the surface, but reaching a maximum some distance away beyond which it falls off with depth. The maximum occurs at

$$\xi_m = -\frac{1}{c_1}$$

with the value

$$K_{*\max} = -\frac{k\xi_m}{e}.$$

We showed in M2 that a steady-state solution with the dimensionless eddy viscosity increasing linearly with depth until it reaches a maximum value which it took for greater depths, gave essentially the same result as (5). This suggests that, given u_* and f, there is a maximum mixing length $(=\xi_m u_*/f)$, that governs the scale of turbulent exchange in the outer part of the boundary layer. For the neutral PBL, our previous results indicate that ξ_N (where the subscript N denotes neutral buoyancy) lies in the range -0.15 to -0.20.

Eddy exchange in the PBL is strongly affected by vertical density fluctuations, caused either by surface buoyancy flux associated with the ice melting or freezing, or by a turbulent flux associated with current shear near the top of the pycnocline. We show below that the surface buoyancy flux is probably not large enough to cause appreciable departure from neutral stability under normal drift

conditions, and present a scaling argument to arrive at a plausible eddy viscosity formulation for the upper pycnocline.

In the central Arctic, sea ice keeps the mixed layer always near its freezing point, and the influence of solar heating or radiational cooling is felt mainly as a surface buoyancy flux due to melting or freezing. Melting is dominant under the high sun angles of summer, and introduction of fresh water at the surface will act to suppress turbulence, since the eddies transporting momentum downward must work against a stable density gradient. It is conventional to quantify this tendency with an Obukhov length scale, which in its nondimensional representation is

$$L_* = \frac{fu_*^2}{k\overline{b'w'}},$$

where $\overline{b'w'} = (g/\rho)\overline{\rho'w'}\big|_0$ is the surface buoyancy flux. For fixed fu_*^2, L_* varies inversely as the buoyancy flux, presumably affecting the turbulence at smaller and smaller scales. Since the size of the energy-containing eddies is of order ξ_N in the neutral PBL, it follows that the kinetic energy of the turbulent regime in the outer boundary layer ought to be increasingly affected by buoyancy as the ratio $|\xi_N/L_*|$ approaches or exceeds unity. In other words, as long as L_* is large compared to ξ_N (L_* is infinite under neutral conditions), the turbulence will scale with ξ_N. In order to quantify these concepts, we considered what melting rate would be required for $|\xi_N/L_*|$ equal to unity, with $u_* = 1$ cm s^{-1}, which was typical of summer conditions. We used Eq. (9) of MS to solve for the melting rate required to satisfy the above ratio: it turned out to be of the order 7 cm day^{-1}. The actual melting rate probably averaged 5–10 times smaller (corresponding to a total ablation of ~50 cm over the melt season—more frequent measurements were not made); thus neutral scaling, with $\xi_N = 0.167$, was used.[1]

A far more significant effect of surface melting was the establishment of a secondary pycnocline at ~25 m depth toward mid-July. Its impact on the dynamics was especially apparent in the fact that this event coincided with the appearance of large-amplitude inertial waves in the velocity records from current meters suspended at 30 m. In order to model the eddy viscosity in the stably stratified region just below this interface, we reasoned as follows. We began by leaving intact the idea that eddy viscosity is a product of a turbulent scaling velocity and a mixing length. But in a strongly stable environment, the mixing length ought to be much more a function of the local Obukhov length L_p than of ξ_N. If the magnitude of the local turbulent stress is τ_p and the buoyancy flux is $\overline{b'w'}\big|_p$, then

$$L_p = \frac{\tau_p^{3/2}}{k\overline{b'w'}\big|_p},$$

so we have

$$K_p \propto \tau_p^{1/2} L_p = \frac{\tau_p^2}{k\overline{b'w'}\big|_p}.$$

Further, we assume the buoyancy flux can be related to the mean density gradient by a mass eddy exchange coefficient that is proportional to K_p, whence

$$K_p^2 = \gamma^2 \tau_p^2 / N^2, \tag{6}$$

where

$$N^2 = -\frac{g}{\rho}\frac{\partial \rho}{\partial z}.$$

Thus K_p varies directly with the local turbulent stress and inversely with the strength of the inversion as measured by the buoyancy frequency N. In practice, the turbulent stress at a given level is estimated from the previous time step, and a lower limit on the turbulent eddy viscosity is specified such that it is never less than molecular.

A linear damping is applied at each time step by decreasing the carryover stress from the previous time step by a small factor, which depends on grid size and time step. The damping is required for numerical stability since there is no external forcing besides the surface stress: in a crude way it models turbulent dissipation. The damping factor d_0 and γ constitute the main adjustable parameters of the model; values chosen after some experimentation are $d_0 = 0.012$ and $\gamma = 0.2$ for a time step of 15 min. The grid interval varies with depth, being logarithmic near the surface; 0.5 m from 2 to 30 m depth; and 1 m for depths from 30 to 59 m. Further details of the numerical procedure are presented in the Appendix.

The framework of the model can be made general enough to allow conservation equations for buoyancy and mass, but since mixed-layer characteristics did not vary much over the time period examined (see McPhee, 1978b, Appendix B; also, comments in Section 5), we held its depth constant (25 m) and estimated the buoyancy frequency to be $N = 0.025$ s^{-1}.

The kinematic surface stress used to drive the model is obtained by expressing the stress on the ice undersurface in terms of the measured surface wind and ice mass; i.e., by combining Eqs. (7) and (13) of II, *viz.*,

$$(\rho_w u_* + imfc_\tau e^{-i\beta})\mathbf{u}_* = \rho_a c_{10} U_{10} \mathbf{U}_{10}, \tag{7}$$

where $\mathbf{U}_{10}$ is the 10 m wind, ρ_a air density, c_{10} a

[1] L_* is the inverse of the parameter μ_* often used to classify buoyancy effects in the atmospheric PBL. For the radiationally cooled atmosphere, values of μ_* as high as 200 have been reported (Businger and Arya, 1974). For the period we considered it is doubtful that μ_* exceeded 1.

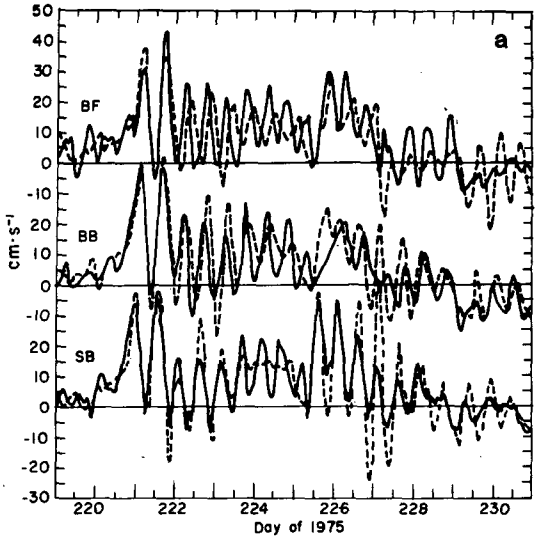

FIG. 4a. Eastward component of simulated surface velocity (dashed curves) superimposed on observed ice drift velocity. Identical model parameters were used for all camps.

constant drag coefficient, m the ice mass per unit surface area, and β and c_τ are functions of the under-surface Rossby number [see Eqs. (14) and (15) of M2]. The kinematic surface stress is $\boldsymbol{\tau} = u_* \mathbf{u}_*$. Values for all the constants are given in M2, as is the surface roughness, $z_0 = 10$ cm.

Implicit in this is the assumption that wind stress passed through the ice is not modified by the inertial motion of the ice itself. The best evidence for this is a lack of inertial energy in the currents measured relative to the drifting ice by meters suspended at 2 m. The mass of the water column between the ice and 2 m is of the same order as the mass of the ice itself. If there were an appreciable modification of the wind stress due to inertial accelerations of the ice, we would expect similar modifications between the interface and the 2 m level, which would imply a larger inertial component in the shear between those levels than was observed. Numerical work solving the equations of motion while carrying ice inertial forces as a dynamic boundary condition (R. Colony, personal communication) also confirmed the hypothesis. While the assumption is not crucial to the model, it simplifies posing the boundary conditions and was used in what follows. The net effect of (7) is to rotate and reduce the wind stress according to a Rossby similarity law appropriate to sea ice. The spectral distribution of the stress is unchanged.

Using winds measured at SB, BB and BF, the model was used to simulate the boundary-layer response at each camp for the 12-day period. In each case, the PBL was assumed to be initially quiescent. Results of the surface velocity simulations are shown in Fig. 4 superimposed on the measured drift. Response to the first episode appears reasonably realistic for the first few inertial cycles at all the camps, but thereafter various changes occur that will be discussed in more detail in the next section. Overall, we were pleased that the multilevel PBL model would predict surface motion as well as (and in the case of phase response at SB, better than) the bulk model of M1.

The other direct tests of the model are shown in Figs. 5 and 6 where the modeled currents at 2 and 30 m are compared with observations. The measurements were made relative to the drifting ice; therefore, the modeled surface velocity has been subtracted from the modeled currents for a direct comparison. In a fixed (to the earth) reference frame, the current at 30 m is small, and the current at 2 m has a strong inertial component. The lack of relative inertial motion between the ice and 2 m is well simulated by the model and lends credence to the notion that momentum transfer near the surface is insensitive to inertial accelerations.

The relatively small absolute inertial component at 30 m in both the model and data shows that direct surface-driven inertial motion is effectively limited to the mixed layer by the steep pycnocline. For a short period beginning about day 227, the observed 30 m current at BB shows considerably less inertial energy than either the ice velocity or the simulation. This event, which happened only at BB, probably coincided with a temporary deepening of the mixed layer.

A "slab" model introduced by Pollard and Millard (1970) has been used, often with considerable success, to simulate observations of inertial currents

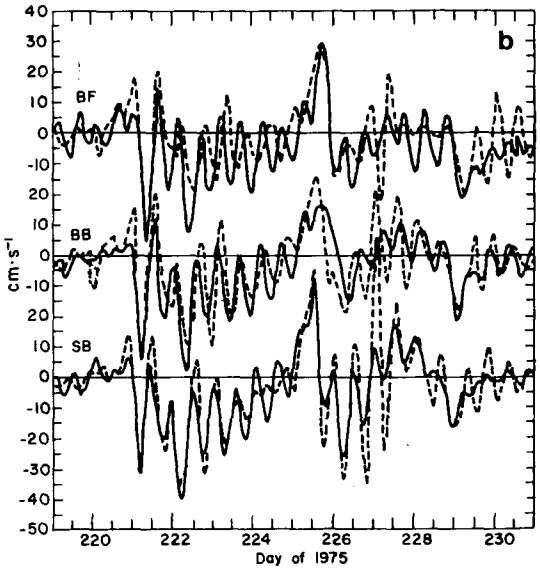

FIG. 4b. As in Fig. 4a except for northward component.

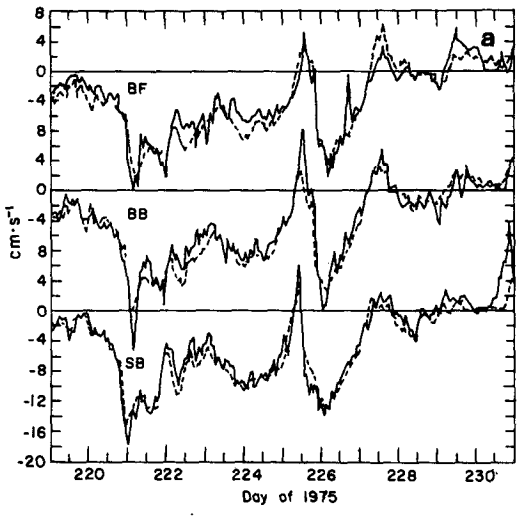

FIG. 5a. Eastward component of simulated current at 2 m depth, *relative to surface*, superimposed on measured currents.

in the mixed layer [e.g., see also Kundu (1976) and Blackford (1978)]. The essential principle is that the integrated inertia (including Coriolis and local time-derivative accelerations) just balances the applied surface stress less a small damping term. The approach is thus integral in depth as opposed to the differential stress equation solved here. In order to interpret actual current records, it is further assumed that velocity in the mixed layer is uniform, equal to the total transport divided by mixed-layer depth, hence the appellation "slab." (In M1 we dropped the slab assumption.)

While the idea of uniform velocity is clearly suspect near the surface, our model results suggest that the two approaches are not incompatible for

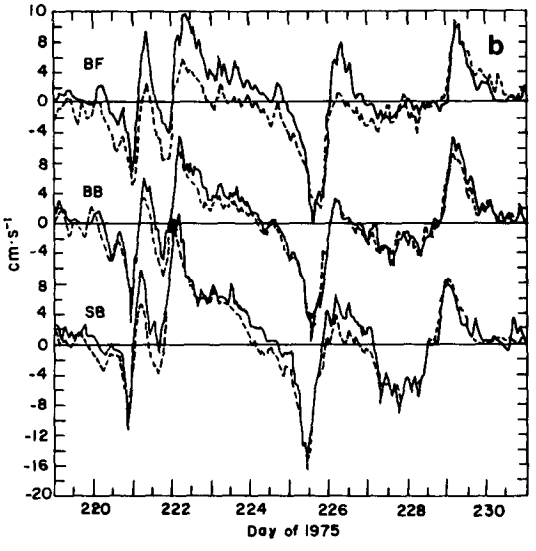

FIG. 5b. As in Fig. 5a except for northward component.

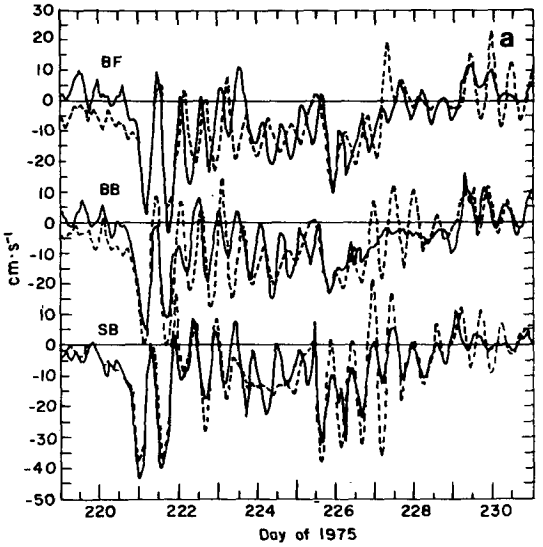

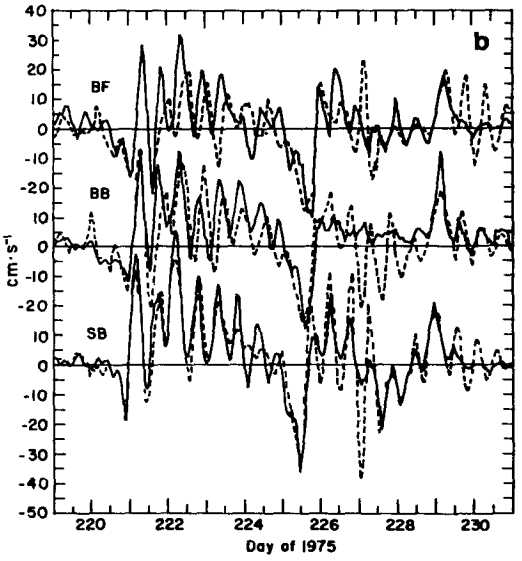

FIG. 6. As in Fig. 5 except for relative currents at 30 m depth.

predicting interior mixed-layer currents, at least for relatively thin layers. Fig. 7 shows velocity components at four levels calculated from BB winds. The dashed curves were obtained by convolving the series with a 12 h Hanning-type filter. Also, shown is the "average" current obtained by integrating the calculated velocity divided by the mixed-layer depth. Deviation of the currents at 10 m and 20 m from the averaged transport is small; thus the main body of the layer appears slablike in the model. Stress (the variable actually modeled) does, of course, vary significantly through the mixed layer as shown by Fig. 8.

The existence of large shear across the pycnocline does not necessarily imply correspondingly large turbulent activity there. In the model, the shear

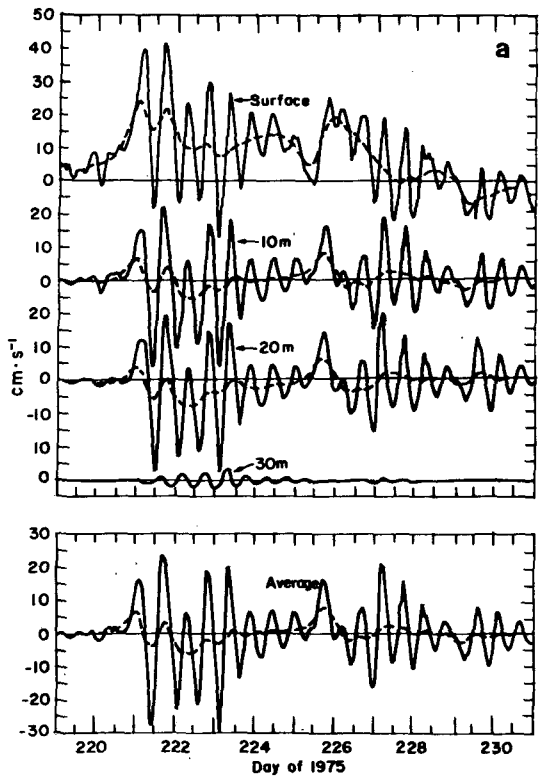

FIG. 7a. Eastward component of simulated (using BB wind) currents at four levels, along with approximate "average" obtained by dividing integrated velocity by mixed-layer thickness. Broken curve results from smoothing with 12 h Hanning-type filter.

results from dividing relatively small stress values, which are in phase from level to level, by even smaller K values. This point is illustrated by using the model as forced by BB winds to examine the shear production of turbulent kinetic energy (TKE). Fig. 9a shows the magnitude of the mean flow shear at 2 m and at 26 m, 1 m below the density interface. Fig. 9b shows corresponding series of the quantity

$$\tau^x \frac{\partial \hat{u}}{\partial z} + \tau^y \frac{\partial \hat{v}}{\partial z} = [(\tau^x)^2 + (\tau^y)^2]/K_m, \qquad (8)$$

which is proportional to the rate per unit volume at which energy of the mean flow is lost through turbulence. Thus, while shear near the top of the pycnocline is several times that at 2 m, the TKE production by shear is an order of magnitude smaller. In the strongly stable environment of the pycnocline, the shear production is partitioned into turbulent dissipation and a work term proportional to the upward buoyancy flux; the point here is that large shear is not necessarily associated with rapid entrainment.

A related question is: since most of the shear in the inertial component of velocity occurs in the upper few meters of the pycnocline (see Fig. 7), how important is inertial oscillation to TKE production near the interface? Recall that most of the year, the ice pack quells inertial motion, even though it often moves freely on synoptic scales. Does the lack of inertial motion (which makes the winter ice/ocean PBL more analogous to the atmospheric PBL) cause a dramatic change, for example, in the entrainment rate at the density interface? In practical terms, is it necessary to resolve inertial motion to study the long term evolution of the ice/ocean PBL? We approached the question by considering a time-independent set of equations that was otherwise as close as possible to the model described above. The K distribution in the pycnocline was determined by, first estimating the stress at the interface for use in (6), then iteratively solving for and substituting the interfacial stress until its change from one iteration to the next was below a specified tolerance. Fig. 10 shows one component of surface velocity obtained by solving the steady problem at hourly intervals, superimposed on the time-dependent results (including the smoothed curve) from Fig. 7. Fig. 11a shows TKE production (Eq. 8) according to each model, along with its time integral (proportional to work per unit volume done by turbulent shear) at 26 m. While these treatments undoubtedly oversimplify the physics of the pycnocline, they hint, on the one hand, that inertial oscillations may enhance turbulent mixing; but on the other, that resolution of inertial mo-

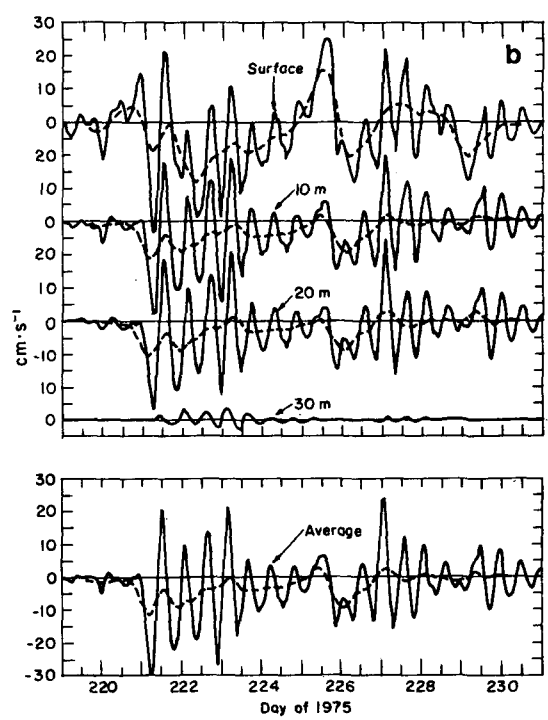

FIG. 7b. As in Fig. 7a except for northward component.

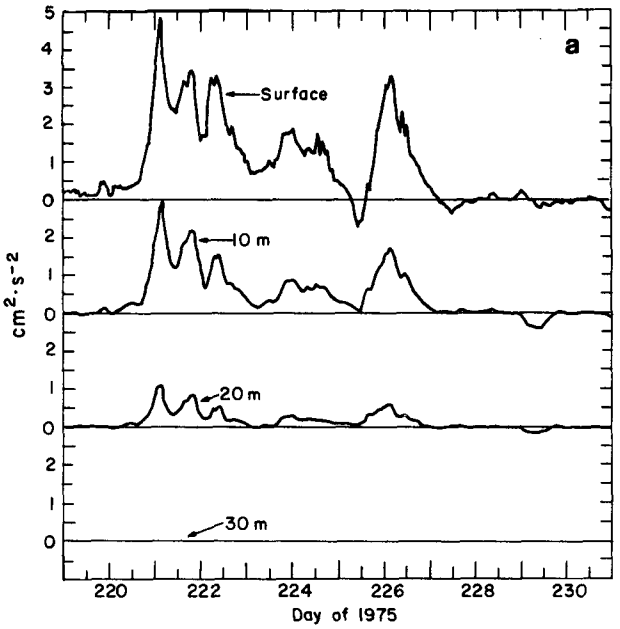

FIG. 8a. Eastward component of simulated kinematic stress at four levels, as driven by BB wind.

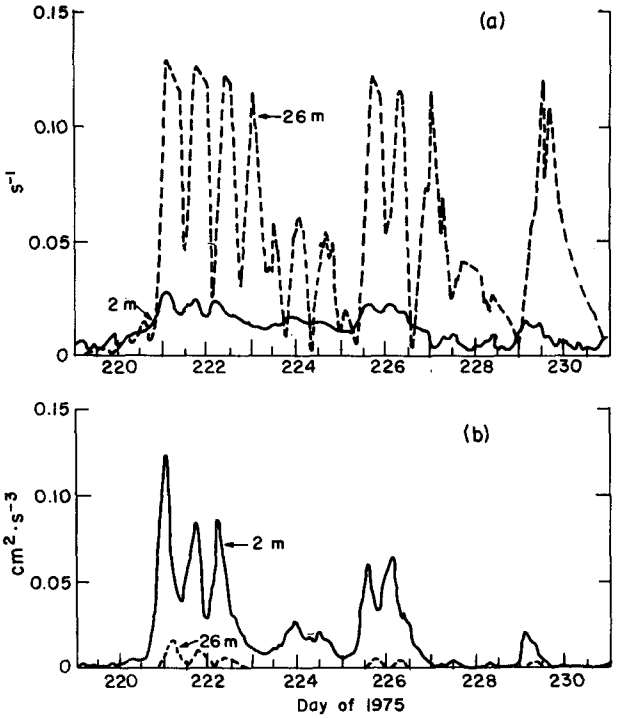

FIG. 9. Velocity shear ($|\tau|/K_m$) near surface and near top of pycnocline, simulated from BB wind (a) and shear production of TKE at same levels (b).

tion may not be required for credible estimates of interfacial mixing. Obviously, a set of careful measurements, which would appear to be feasible in the Arctic, would be useful for settling this point.

4. Spatial variations

In order to describe the inertial part of the velocity field, particularly its horizontal variation, it is convenient to employ a shorthand introduced by Perkins (1970) in which a complex waveform is fit to the observed velocity over some interval such that the least-squares difference between the waveform and the actual velocity is minimized; i.e., over time interval $2T$ the velocity

$$\mathbf{u} = u + iv$$

is fit with a complex wave

$$\mathbf{A}e^{-ift} = Ae^{i(\phi - ft)},$$

where $\mathbf{A}$ is a complex constant (over the interval $2T$) of amplitude A and phase ϕ. The discrete

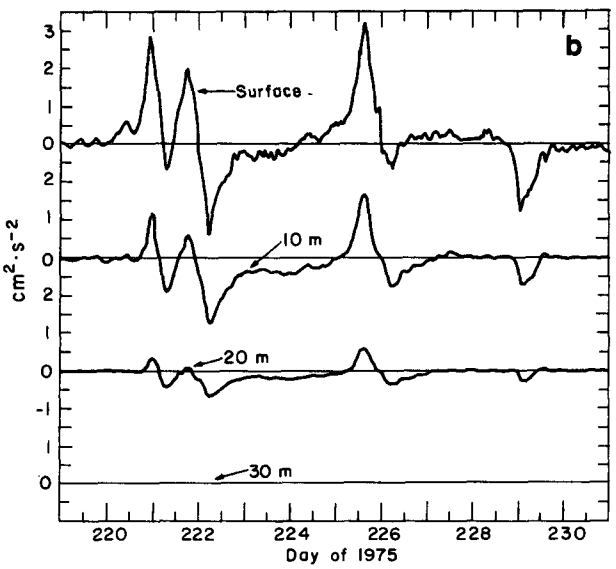

FIG. 8b. As in Fig. 8a except for northward component.

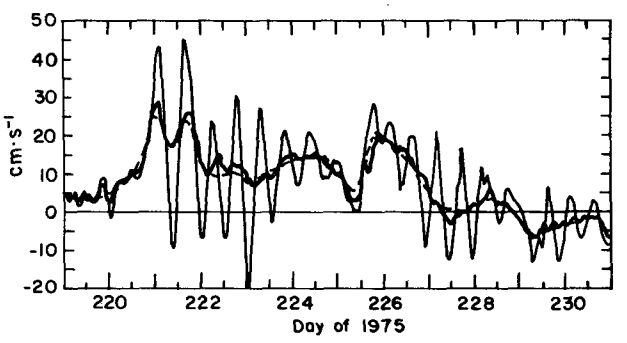

FIG. 10. Simulated eastward component of surface velocity at BB. Heavy solid curve shows hourly solutions of steady-state PBL model; light solid curve is time-dependent solution; dashed curve shows time-dependent solution smoothed with 12 h filter.

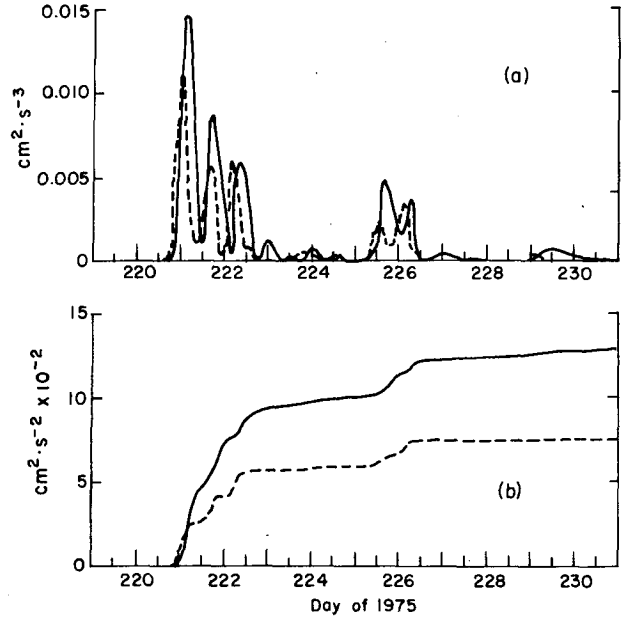

FIG. 11. (a) Comparison of rate of shear production of TKE according to time dependent model (solid) and hourly solutions of steady-state model (dashed); and (b) time integrals of curves in (a).

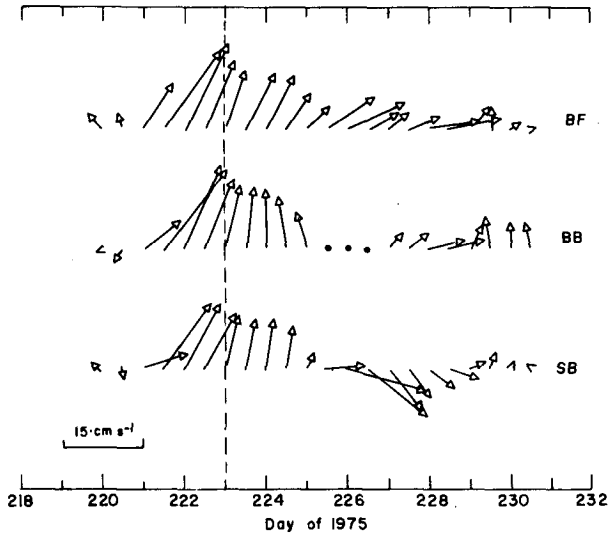

FIG. 13. As in Fig. 12 except constant travel-time phase adjustments at SB and BB as described in text.

calculation is equivalent to computing the Fourier coefficient over a relatively short time interval, so that if nearby spectral peaks are present, a suitable filter should be used (see, e.g., Kundu, 1976). Since tides are weak in the Arctic, and at any rate, the principal tidal component (M_2) is too close to separate from the inertial frequency at the ice stations, we performed the direct calculation, which was to fit the complex waveform in a least-squares sense to the velocity time series over an interval $2T = 24$ h.

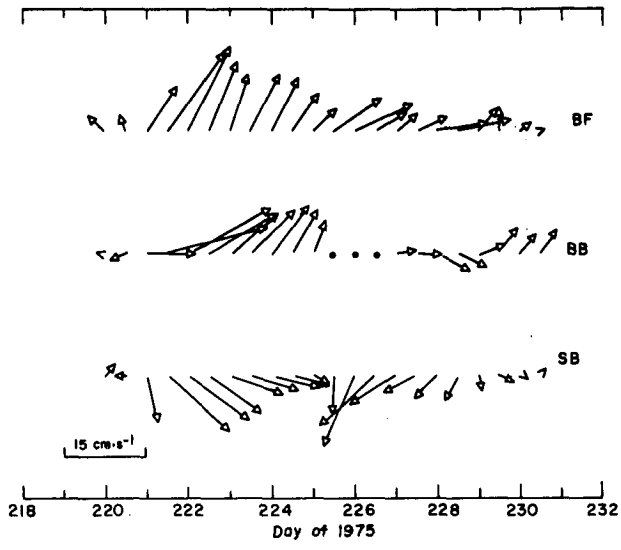

FIG. 12. Complex waveform coefficients fit to drift velocity data, represented as polar vectors. Phase angle is positive counterclockwise from horizontal (time) axis.

Complex coefficients were calculated from the velocity series of each of the camps every 12 h from the preceding and succeeding 12 hourly samples. The total interval was close to twice the inertial period conforming with Perkins' (1970) treatment.

A can be represented as a polar vector of length A at an angle ϕ counterclockwise from an axis dependent on the choice of $t = 0$. An idealized circular, inertial oscillation of constant amplitude would thus appear as a train of parallel vectors of equal length. Actual waveform coefficients as calculated for the three camps are shown in Fig. 12. Values at BB for the period 225.5–226.5 have been deleted because of NAVSAT sampling problems.

For the first part of the record, the coefficients are remarkably similar in magnitude and relative orientation across the array. This is perhaps made clearer by considering two sites that experience inertial motions which are identical except that the forcing occurs a few hours later at the second site. For concreteness, suppose that the oscillation at site 1 is $\mathbf{A}_1 e^{-ift}$ and at site 2 it occurs one-quarter of an inertial period (roughly 3 h) later, i.e., $\mathbf{A}_2 e^{-if(t+\pi/2f)}$. It follows that $\mathbf{A}_2 = \mathbf{A}_1 e^{i\pi/2}$, so at site 2 the complex coefficient has rotated by 90°. A disturbance moving eastward at $V_f = 60$ km h^{-1} would cross the array in 3.36 h, slightly more than a quarter of an inertial period. In Fig. 13, all the coefficients for SB and BB have been rotated through an angle $f\Delta x/V_f$, where Δx is the zonal distance from each camp to BF. In the first half of the record, the amplitude changes very little across the 190 km array and the phase shift is small when

adjusted by a simple arrival time argument. The second half is not so well behaved. The inertial signal at BF lags that at SB by almost 180° on day 227.5, which is consistent with the observation that the second disturbance moved about half as fast, say, 30 km h^{-1}. But note from Fig. 13 that the phase difference between BB and BF during the period 227–229 implies V_f = 60 km h^{-1}. During the same period there is also more variability in the amplitude from camp to camp, with generally lower levels of inertial energy. This suggests that in the second half, horizontal gradients in the wind, which we would expect to be sharper, played a more important role.

Evaluating how well a model can reproduce a particular observed event is seldom a straightforward task. The primary test of the model presented here has been how well it can predict surface drift, both at synoptic and inertial frequencies. Fig. 4 indicates that the model does quite well on the longer term drift, as might be expected from the results of M2. The quality of the inertial response is not quite so clear. Certainly, the simulated magnitude of the first few oscillations is respectable, but note the phase drift after just a few periods at BF. In the second half of the 12-day interval, the modeled amplitudes tend to be somewhat large, particularly at SB around day 227.

Problems with phase response are shown more clearly in Fig. 14, which is analogous to Fig. 13 except that model output has been used to calculate the complex coefficients. Note that the coefficients again have been rotated at SB and BB by assuming that the storm events travel eastward at 60 km h^{-1}. Fig. 14 compared to Fig. 13 thus indicates how well the inertial components are modeled, both in magnitude and phase.

In general, the discrepancy between observed and simulated response is caused either by failure of the model to properly treat the physics it purports to include, or because some neglected physical process, in fact, is important. Under the former class, likely candidates in our case might be the treatment of eddy viscosity in the upper pycnocline or the crude way in which dissipation is approximated by linear damping. We found through parameter studies that the phase response as the inertial trains decayed was sensitive to both γ and d_0: these parameters were adjusted to give the response shown at SB and then held constant. It should be noted, however, that prediction of the first three or four cycles in each episode were relatively insensitive to changes in γ or d_0. Moreover, examination of Fig. 14 suggests that improvement in treatment of physical processes within the locally driven model, in any event, is unlikely to produce the alignment apparent in the first half of Fig. 13 at all the camps. Consider the complex coefficients on day 223. In Fig. 13, with an arrival

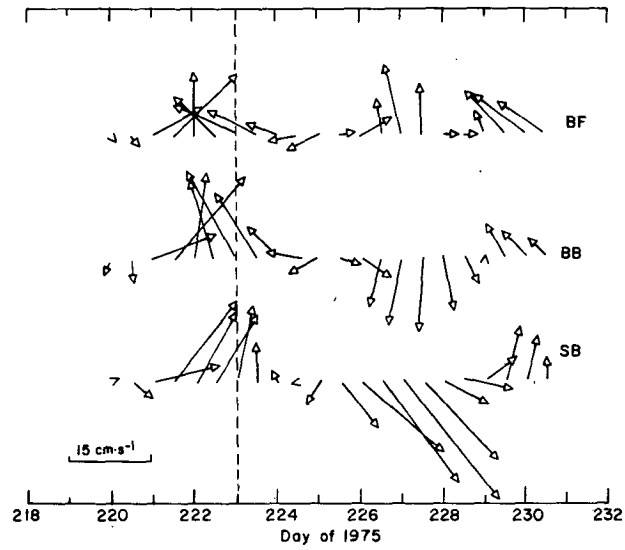

FIG. 14. As in Fig. 13 except simulated data. Phase at SB and BB is adjusted for arrival time assuming 60 km h^{-1} front propagation.

time phase adjustment, the coefficients are nearly identical. In Fig. 14, the coefficients produced by different observed winds driving the same model show a substantial phase shift across the array. Note also the observed phase alignment at BF for almost the entire period. In contrast, the numerical results for BF show a rapid phase change soon after the first front has passed that is not present in the SB simulation. Thus details of the moving wind system have changed from SB to BF.

The fact that observed response (for the first half) is so similar at the three stations implies some coupling mechanism in addition to the wind. Obviously, the moving wind front provides the main motive force exciting the inertial oscillations, but it also appears that the ocean adjusts so as to modify the forcing. This is not unexpected. As W. Krauss has shown, using first a two-layer model (Krauss, 1972) and subsequently a continuously stratified model (Krauss, 1976), horizontal gradients in the wind stress, which cause PBL transport divergence and consequent vertical velocities, can force inertio-gravity waves at depth, in spite of a lack of frictional coupling between the surface and deep ocean. Such motions are observed quite regularly (e.g., Perkins, 1970). Krauss' treatments assume the upper surface to have no vertical motion with a constant-pressure boundary condition, which forces the mixed layer to follow the local wind. But suppose that some small part of the vertical velocity in the mixed layer were to raise the sea surface; then a local pressure term would affect the PBL dynamics. While a rigorous three-dimensional approach to this problem seemed be-

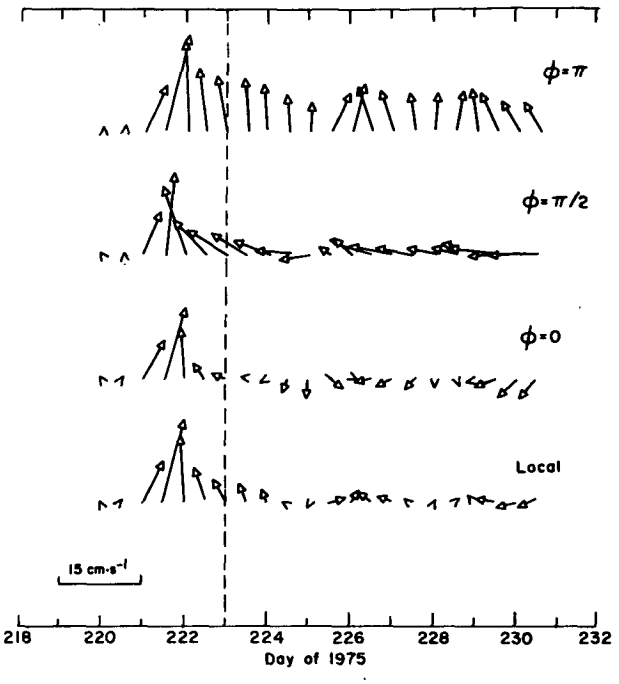

FIG. 15. Complex wave form coefficients for simulations of transport at BF using bulk model described in text including simplified interaction term. Series marked "local" had no interaction; others used $\alpha = 0.05$. All had damping time constant of six inertial periods.

yond the scope of this paper, we carried out a simple heuristic exercise that qualitatively showed some of the observed characteristics and is outlined below.

We consider first a step-function front propagating zonally with speed V_f that excites purely local inertial oscillations having the form (after the front has passed)

$$\mathbf{M}_I = \mathbf{M}_0 \exp[i(\lambda x - ft)],$$

where $\mathbf{M}_I$ is the integrated inertial transport, $\mathbf{M}_0$ a complex constant and λ a wavenumber related to V_f, *viz.*,

$$\lambda = \frac{f}{V_f} = \frac{2\pi}{L}, \qquad (9)$$

and L is the wavelength over which the inertial pattern repeats itself spatially. The time rate of change of mixed-layer thickness is

$$\frac{\partial \zeta}{\partial t} = -\nabla \cdot \mathbf{M}_I$$

and in the idealized case at $x = 0$, the gradient of mixed-layer thickness would be

$$\frac{\partial \zeta}{\partial x} = \frac{\lambda^2 M_0}{f} \sin(\phi - ft),$$

where M_0 is the magnitude of inertial transport and ϕ is a phase angle. Now if some fraction of the change in ζ occurs as sea surface elevation or depression (i.e., $\Delta\eta = \alpha\Delta\zeta$), we have an integrated pressure gradient force acting on the mixed layer in the zonal direction, i.e.,

$$F_x = -\frac{g\alpha H\lambda^2}{f} M_0 \sin(\phi - ft),$$

where H is the mixed-layer depth and g the acceleration of gravity. In reality, α and ϕ probably change rapidly as the ocean adjusts (i.e., as energy is propagated downward by inertio-gravity waves), and the wind field would properly be characterized by a whole wavenumber spectrum. Despite this, we investigated the small surface elevation aspect of the problem by using the observed wind at BF to drive a simple slab model similar to that of Pollard and Millard (1970) except for the term F_x. Holding α and ϕ constant, we solved the equation

$$\frac{\partial \mathbf{M}}{\partial t} + if\mathbf{M} = \tau_s + F_x - \left(\frac{f}{2\pi N}\right)\mathbf{M}, \qquad (10)$$

where $\mathbf{M}$ is the total PBL transport, τ_s the surface stress as before, and N the damping time expressed in inertial periods. Using $N = 6$, $\lambda = (2\pi/750)$ km^{-1} and $H = 25$ m, Eq. (10) was solved first with $\alpha = 0$ for a local simulation; then with $\alpha = 0.05$ and ϕ successively 0, $\pi/2$, and π. For each 15 min time step, M_0 was estimated by subtracting the steady-state transport ($i\tau_s/f$) from calculated transport at the previous time step.

The resulting series were analyzed at the inertial period as above and the complex coefficients (divided by H) are plotted in Fig. 15. We stress that the purpose here is not to directly simulate surface motion, but rather to see whether one extremely simplified aspect of oceanic coupling could produce the observed phase alignment when driven by actual local forcing. The results, particularly in the cases when $\phi = \pi/2$ and $\phi = \pi$, indicate that it can. As the expression for F_x depends on the square of the wavenumber; the slower propagation of the second event would be relatively more important and might account for both the poorer agreement of the simulations and the diminished coherence in the data. This interpretation suggests that for primary wavelengths [as defined by Eq. (9)] of the order 750 km or greater, the interference is small and may be constructive in the sense that the oscillations are aligned and preserved by the oceanic coupling. At wavelengths shorter by a factor of 2, the interference appears to be mainly destructive.

It is not clear to what degree this behavior is attributable to mechanical forces within the ice cover itself as opposed to the PBL divergence discussed above. Even at its lowest concentration, sea ice covers most of the central Arctic Ocean,

and there are persistent historical reports of inertial (or perhaps tidal) periods in ice deformation (although we know of none pertaining directly to the melt season). Therefore, a plausible argument can be made that ice causes local changes in the momentum balance, and that the interaction scales found here are appropriate only to an ice-covered ocean. Unfortunately, we do not see how this question can be resolved with the present data.

5. Summary

This paper presents the second application of a relatively simple first-order PBL theory to describe momentum transfer in the upper ocean. In the first instance (M2), we used it to explain statistical properties of the surface stress and velocity fields, ignoring components of motion at inertial or higher frequencies. In this work, we have attempted to simulate directly the response of the boundary layer during specific wind events. Since inertial oscillations are a prominent aspect of that response, we have discussed in some detail both their simulation by the locally forced model, and their horizontal structure across the 190 km array of drifting stations. While the model cannot reproduce precisely the observed inertial motion, we feel that the response of the whole array indicated a coupling that cannot be properly accounted for without considering horizontal gradients. But this appears to be a secondary effect as far as the general problem of PBL momentum transfer is concerned, and we consider the overall performance of the horizontally homogeneous model to be quite good.

We have purposely steered away from treating this formulation as an entrainment model, mainly for the reason that from the AIDJEX camps, especially during the summer of 1975, small scale (~10 km) events were observed frequently in which isopycnal levels throughout the upper 300 m of the water column rose and fell quite rapidly (McPhee, 1979b). Similar features were seen in 1972 and subsequently shown to have a controlling influence on short term mixed-layer characteristics (McPhee, 1975). Until further assessment of what impact these have on mixed-layer evolution is made, it seems fruitless, and perhaps misleading, to attempt local (one-dimensional) entrainment modeling.

This and two other papers (MS and M2) reinforce the hypothesis that a conceptual framework developed mainly for the atmospheric PBL can be used to successfully interpret the oceanic PBL. In this respect, our results complement those of Mellor and Durbin (1975). The relationship of their "level-2" model to the more complex "level-4" model described by Mellor and Yamada (1974) is somewhat paralleled by the Businger and Arya approach having its antecedents in the second-order closure work of Wyngaard *et al.* (1974) and the numerical integrations of Deardorff (1972). In each case, a simplification consistent with Rossby-number similarity is obtained, using the important concept that the mixing length for turbulent exchange is constantly scaling itself to turbulence levels in the flow. The main question remaining in extending the atmospheric results to the ocean (and vice versa) seems to be how PBL turbulence behaves in the presence of density gradients *and* inertial oscillations. Obviously, a properly controlled experiment measuring mean flow and turbulence near a density interface in a real geophysical flow is not an easy undertaking; nevertheless, the AIDJEX experience indicates that such a project is feasible from pack ice in summer.

Acknowledgments. R. Colony developed a major part of the numerical technique for the model, and W. D. Hibler III provided valuable assistance and suggestions for improving the manuscript. Their help is gratefully acknowledged. The work was supported by the National Science Foundation under Grant DPP 77-17341.

APPENDIX

The Numerical Technique

The numerical technique is as follows: Let the horizontal stress vector at level i and time step j be denoted

$$\phi_{i,j} = \begin{pmatrix} \tau^x_{i,j} \\ \tau^y_{i,j} \end{pmatrix}.$$

We now define

$$\alpha_i = \frac{1}{\Delta z_i} = \frac{1}{z_{i+1} - z_i},$$

$$\beta_i = f(\Delta z_{i-1} + \Delta z_i)/(8K_{i,j+1}),$$

$$\gamma_i = (\Delta z_{i-1} + \Delta z_i)/(4\Delta t K_{i,j+1}),$$

where Δt is the time step. The matrix equation at each new time step $(j + 1)$ for each level is given by

$$A_i\phi_{i-1,j+1} + B_i\phi_{i,j+1} + C_i\phi_{i+1,j+1} = D_i, \quad \text{(A1)}$$

where

$$A_i = \begin{pmatrix} -\alpha_{i-1} & 0 \\ 0 & -\alpha_{i-1} \end{pmatrix},$$

$$B_i = \begin{pmatrix} \gamma_i + \alpha_i + \alpha_{i-1} & -\beta_i \\ \beta_i & \gamma_i + \alpha_i + \alpha_{i-1} \end{pmatrix},$$

$$C_i = \begin{pmatrix} \gamma_i - \alpha_i & -\beta_i \\ \beta_i & \gamma_i - \alpha_i \end{pmatrix},$$

$$D_i = (1 - d_0)\begin{pmatrix} \gamma_i & \beta_i \\ -\beta_i & \gamma_i \end{pmatrix}(\phi_{i+1,j} + \phi_{i,j}),$$

where d_0 is a small damping, equivalent to a linear drag.

The simultaneous algebraic equations (A1) are solved by standard tridiagonal matrix reduction, i.e.,

$$\phi_i = F_i - E_i\phi_{i+1}, \quad i = 1, N-1,$$

where

$$\left.\begin{aligned} F_i &= (B_i - A_iE_{i-1})^{-1}(D_i - A_iF_{i-1}) \\ E_i &= (B_i - A_iE_{i-1})^{-1}C_i \end{aligned}\right\} i = 2, N.$$

F_1 is the applied surface stress; $\phi_N = 0$. The implicit scheme involves inversion of a 2×2 matrix, which makes it relatively efficient.

Velocity may be obtained at any time by integrating the stress profile from depth.

REFERENCES

Blackford, B. L., 1978. Wind-driven inertial currents in the Magdalen Shallows, Gulf of St. Lawrence. *J. Phys. Oceanogr.*, **8**, 653–664.

Businger, J. A., and S. P. S. Arya, 1974. The height of the mixed layer is a stably stratified planetary boundary layer. *Advances in Geophysics*, Vol. 18A, Academic Press, 73–92.

Deardorff, J. W., 1972. Numerical investigations of neutral and unstable planetary boundary layers. *J. Atmos. Sci.*, **29**, 91–115.

Kondo, J., Y. Sasano, and T. Ishii, 1979. On wind-driven current and temperature profiles with diurnal period in the oceanic planetary boundary layer. *J. Phys. Oceanogr.*, **9**, 360–372.

Krauss, W., 1972. Wind-generated internal waves and inertial period motions. *Dtsch. Hydrogr. Z.*, **25**, 241–250.

——, 1976. On currents, internal and inertial waves in a stratified ocean due to variable wind fields. Part 1. *Dtsch. Hydrogr. Z.*, **29**, 87–96.

Kundu, P. J., 1976. An analysis of inertial oscillations observed near Oregon Coast. *J. Phys. Oceanogr.*, **6**, 879–893.

McPhee, M. G., 1975. The effect of ice motion on the mixed layer under Arctic pack ice. *AIDJEX Bull.*, No. 30, 1–27 [NTIS PB28-8574].

——, 1978a. A simulation of inertial oscillation in drifting pack ice. *Dyn. Atmos. Oceans*, **2**, 107–122.

——, 1978b. AIDJEX Oceanographic Data Report. *AIDJEX Bull.*, No. 39, 33–78.

——, 1979a. The effect of the oceanic boundary layer on the mean drift of pack ice: Application of a simple model. *J. Phys. Oceanogr.*, **9**, 388–400.

——, 1979b. An analysis of pack ice drift in summer. Paper presented at *A Symposium on Sea Ice Processes and Models*, Seattle, Proceedings to be published by University of Washington Press.

——, 1979b. Unpublished manuscript. Some thoughts and a few data on modelling and prediction of the upper layers of the ocean. *Ocean Modelling*, No. 20 (February).

——, 1980: An analysis of pack ice drift in summer. *Sea Ice Processes and Models*, R. Pritchard, Ed., University of Washington Press, 62–75.

——, and J. D. Smith, 1976. Measurements of the turbulent boundary layer under pack ice. *J. Phys. Oceanogr.*, **6**, 696–711.

Mellor, G. L., and T. Yamada, 1974: A hierarchy of turbulent closure models for planetary boundary layers. *J. Atmos. Sci.*, **31**, 1791–1806.

—— and P. A. Durbin, 1975. The structure and dynamics of the ocean surface mixed layer. *J. Phys. Oceanogr.*, **5**, 718–728.

Perkins, H., 1970: Inertial oscillations in the Mediterranean. Ph.D. thesis, MIT-Woods Hole, 155 pp.

Pollard, R. T., and R. C. Millard, Jr., 1970: Comparison between observed and simulated wind-generated inertial oscillations. *Deep-Sea Res.*, **17**, 813–821.

Smith, J. D., 1974: Turbulent structure of the surface boundary layer in an ice-covered ocean. *Proc. 1973 ICES Symp. Physical Processes Responsible for the Dispersal of Pollutants in the Sea, with Special Reference to the Near Shore Zone. Rapport Proces-Verbaux Ser.*, J. W. Talbot and G. Kullenberry, Eds., 55–65.

Thorndike, A. S., and J. C. Cheung, 1977: AIDJEX measurements of sea ice motion, 11 April 1975 to 14 May 1976. *AIDJEX Bull.*, No. 35, 1–149.

Wyngaard, J. C., O. R. Coté and K. S. Rao, 1974: Modeling the atmospheric boundary layer. *Advances in Geophysics*, Vol. 18A, Academic Press, 193–212.